Journal of Power Sources 247 (2014) 57–69

Contents lists available at ScienceDirect

Journal of Power Sources

journal homepage: www.elsevier.com/locate/jpowsour

Significant impact on cathode performance of lithium-ion batteries by precisely controlled metal oxide nanocoatings via atomic layer deposition

Xifei Li [a], Jian Liu [a], Xiangbo Meng [a], Yongji Tang [a], Mohammad Norouzi Banis [a], Jinli Yang [a], Yuhai Hu [a], Ruying Li [a], Mei Cai [b], Xueliang Sun [a,*]

[a] Nanomaterials and Energy Lab, Department of Mechanical and Materials Engineering, University of Western Ontario, London, Ontario N6A 5B9, Canada
[b] General Motors R&D Center, Warren, MI 48090-9055, USA

HIGHLIGHTS

- ALD derived metal oxide (TiO_2, ZrO_2, Al_2O_3) coatings were successfully performed.
- Coatings could significantly increase battery performance of the commercial $LiCoO_2$.
- Al_2O_3 coating brings the best cycling stability.
- ZrO_2 coating contributes to the best rate capability.

GRAPHICAL ABSTRACT

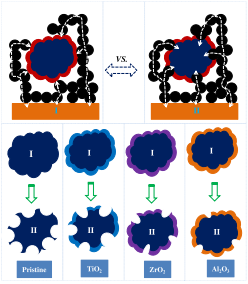

ARTICLE INFO

Article history:
Received 29 May 2013
Received in revised form
8 August 2013
Accepted 16 August 2013
Available online 29 August 2013

Keywords:
$LiCoO_2$ cathode
Atomic layer deposition
Metal oxide coatings
Lithium ion batteries
Cobalt dissolution

ABSTRACT

$LiCoO_2$ in the commercial lithium ion batteries has been suffering from its poor cycling performance at high cutoff voltages. In this study, we employ an atomic layer deposition (ALD) technique to surface-modify a $LiCoO_2$ material with various thickness-controlled metal oxide (TiO_2, ZrO_2 and Al_2O_3) coatings to improve its battery performance. The effects of the metal oxide coatings on the electrochemical performance of $LiCoO_2$ electrode are studied in detail. It is demonstrated that a uniform and dense coating via the ALD route on $LiCoO_2$ powder can lower the battery performance due to an obvious decrease in lithium diffusion and electron transport with the coating layers. In contrast, it is revealed that a direct coating on prefabricated $LiCoO_2$ electrodes performs much better than a coating on $LiCoO_2$ powders. It is further disclosed that the improved electrochemical performance of coated $LiCoO_2$ electrode is highly dependent on the coating materials. Of the three coating materials, the Al_2O_3 coating results in the best cycling stability while the ZrO_2 coating contributes to the best rate capability. It is thus suggested that the coating materials are functionally specific, and for the best improvement of a cathode, a particular coating material should be sought.

1. Introduction

Various lithium transition metal oxides (such as $LiCoO_2$, $LiNiO_2$, $LiCo_xNi_{1-x}O_2$, $LiMn_2O_4$, $LiFe(Mn)PO_4$, $LiNi_{1/3}Mn_{1/3}Co_{1/3}O_2$, etc) have been successfully employed as cathodes in rechargeable lithium ion batteries (RLIBs) since the first commercialized RLIBs by SONY in 1991 [1–3]. $LiCoO_2$, proposed by Goodenough et al. in 1980, [4] is the first commercialized cathode material in RLIBs [5,6], and has been considered as one of the most attractive cathodes due to its ease of production and superior battery performance including high energy density and high working potential (~3.9 V vs. Li/Li^+ couple) [7–9]. As an important cathode in RLIBs, the α-$NaFeO_2$

* Corresponding author. Tel.: +1 519 661 2111x87759; fax: +1 519 661 3020.
E-mail address: xsun@eng.uwo.ca (X. Sun).

0378-7753/$ – see front matter
http://dx.doi.org/10.1016/j.jpowsour.2013.08.042

layer-structured $LiCoO_2$ (space group-R3m, a = 2.815–2.816 Å, c = 14.05–14.08 Å) with oxygen in a cubic close-packed arrangement is composed of consecutively arranged Li^+ and Co^{3+} ions. Moreover, octahedral LiO_6 and CoO_6 share common edges between the layers in the unit cell of $LiCoO_2$ [7,10,11]. To reduce the cathode material size into the nanoscale is an important approach to increase cycling performance [9,12–17]. For example, nanostructured $LiCoO_2$ cathodes (representatively including nanoparticles [16], nanowires [17], and nanosheets [9], etc.) provide shortened diffusion pathway for lithium ion insertion/extraction and electron transport. In addition, the increased surface-to-volume ratio of nanostructured $LiCoO_2$ facilitates lithium ion accessibility from the electrolyte with higher efficiency over bulk $LiCoO_2$ [18]. However, the larger surface area of nanostructured $LiCoO_2$ often results in a heavier formation of solid electrolyte interphase (SEI) in comparison to its bulk counterparts. As a result, nanostructured $LiCoO_2$ is inevitably accompanied by the production of more heat [19]. In addition, a thicker SEI layer leads to deteriorated rate capabilities at high rates, due to its low electrical conductivity as a lithium-ion barrier [20]. Even worse, nanostructured $LiCoO_2$ suffers from its poor tap density, leading to the low RLIB energy density. In contrast, micron-sized $LiCoO_2$ cathode mitigates somewhat the above-discussed challenges, and shows more practical in commercial RLIBs. But, how to further increase battery performance of micron-sized $LiCoO_2$ cathode has been a crucial challenge in the RLIB development.

$LiCoO_2$ cathode exhibits a theoretical capacity of 272 mAh g^{-1}. However, when the battery is charged a cutoff voltage up to 4.2 V, only half lithium is extracted from $LiCoO_2$ to $Li_{0.5}CoO_2$, resulting in the limited capacity (only ~140 mAh g^{-1}) in practical applications [21]. Thus, it is a well accepted strategy to charge $LiCoO_2$ cathode beyond 4.2 V, in order to utilize more lithium ions from the cathode and to increase the specific capacity and the energy density of $LiCoO_2$ [22,23]. However, previous studies also revealed that the inevitable moisture in the RLIB electrolyte could induce $LiPF_6$ decomposition and form HF acid, described as following [24]:

$$LiPF_6 \rightarrow LiF\downarrow + PF_5 \quad (1)$$

$$PF_5 + H_2O \rightarrow POF_3 + 2HF \quad (2)$$

$$2POF_3 + 3Li_2O^- \rightarrow 6LiF\downarrow + P_2O_5\downarrow \quad (\text{or } Li_xPOF_y) \quad (3)$$

The formed HF acid aggravates the dissolution of $LiCoO_2$ cathode, moreover, the charge cutoff voltage over 4.2 V incurs the dissolution of $LiCoO_2$ into the electrolyte, thereby causing an increased capacity fade upon cycling [23,25,26]. In this context, it is critical to mitigate the capacity fading of $LiCoO_2$ in order to satisfy RLIB application.

The charge–discharge cycling of RLIB cathodes is highly related with their surface chemistry [27], thus surface modification via coating was demonstrated being an effective strategy to decrease the cathode dissolution. To date, many metal oxides (such as TiO_2, ZrO_2, and Al_2O_3 et al.) were successfully reported as surface coatings [28–34]. Their functional roles may present in preventing the cathode materials from their direct contact with the electrolyte, simultaneously maintaining ionic conduction pathways, suppressing the release of oxygen and the phase transition, and decreasing the disorder of cations in crystal sites [35,36]. For example, a mechanothermal process was applied to coat TiO_2 on $LiCoO_2$ cathode to obtain higher cycling performance [28]. The ZrO_2 coated $LiCoO_2$ showed better battery performance than the pristine one at both room temperature and elevated temperature of 55 °C [30]. It was found that the ultra-thin Al_2O_3 coating on $LiCoO_2$ resulted in 250% improvement in reversible capacity in comparison to the bare one [32]. Of three reported different configurations of surface coating, i.e., rough coating, core–shell structure coating and ultra-thin film coating [34], the first one cannot fully coat a cathode material, and the intact area leaves the cathode vulnerable to the reactions with the electrolyte. In comparison, the second choice is successful in fully coating a cathode. Unfortunately, the resultant coatings are often very thick and thereby impede the transport of lithium and electron. Therefore, the ultra-thin film coating as the third choice is commonly regarded as the most promising approach, due to its pinhole-free films with complete protection from the electrolyte [34]. To fulfill last route, recently atomic layer deposition (ALD) is receiving an increasing attention ascribed to its unique capabilities in depositing controllable atomic-level thin films with high quality. A lot of efforts have been focused on ALD-coatings onto cathodes [33,37–42], anodes [43–45], and separator [46] to increase electrochemical performance of RLIBs. In case of deposition of metal oxides, ALD has numerous reports including Al_2O_3, TiO_2, and ZrO_2 etc. on various substrates [33,37–46]. To the best of our knowledge, however, a systematic study of various coating layers (Al_2O_3, TiO_2, and ZrO_2) on the electrodes, in particular from the point of view of electrochemical characterization, is scarce.

In this study, we conducted a systematic comparative investigation on the effects of three metal oxide coatings including TiO_2, ZrO_2, and Al_2O_3 on the electrochemical performance of a commercial $LiCoO_2$ cathode material with micron-size. The controllable coatings were deposited via ALD. In addition, the effects due to coating thickness were also addressed in study. It was demonstrated that the controllable coatings are effective in improving both cycling stability and rate capability of $LiCoO_2$ cathode. More importantly, it was inspired from this study that ALD and its resultant materials may ultimately contribute more for robust and high-efficient RLIBs.

2. Experimental

2.1. Preparation of $LiCoO_2$ electrode

$LiCoO_2$ electrodes were prepared by slurry-casting on Al foils that served as current collectors. The slurry contained 80 wt% the cathode materials (commercial $LiCoO_2$ with the particle size of 3–10 um, as shown in Fig. S1 in Supplementary data), 10 wt% carbon black and 10 wt% poly(vinylidene) fluoride binder in the *N*-methylpyrrolidinone (NMP) solvent. The obtained electrode was dried in a vacuum at 90 °C overnight.

2.2. Metal oxide coatings on $LiCoO_2$ electrode via ALD

Various metal oxides (TiO_2, ZrO_2 and Al_2O_3) were directly coated on the $LiCoO_2$ electrode in an ALD reactor (Savannah 100, Cambridge Nanotechnology Inc., USA). Titanium tetraisopropoxide (TTIP), tetrakis dimethylamido zirconium ($Zr(NMe_2)_4$) and Trimethylaluminum (TMA) were chose as Ti, Zr and Al precursor respectively, while H_2O was used as the oxidizer in three cases. The deposition temperature was set as 85, 100 and 150 °C for TiO_2, ZrO_2 and Al_2O_3, respectively. One ALD cycle was executed with the following six steps: (1) pulsing of the first precursor with t_1 s; (2) a 3.0 s extended exposure of the first precursor to the cathode electrode; (3) purging of residual precursor and any byproducts with t_2 s; (4) pulsing of the second precursor with t_3 s; (5) a 3.0 s extended exposure of the second precursor to the cathode electrode; (6) purging of residual precursor and any byproducts with t_4 s. The ALD sequence was expressed as $t_1 - t_2 - t_3 - t_4$ in short. During an ALD process, the purging time is an important parameter, thus this parameter we used in this study was optimized. For example, as shown in Fig. S2, in a case of TiO_2 coated $LiCoO_2$, when the purging time was set as 5 s,

many small particles can be clearly found due to precursor condensation on the cathode followed by a process of chemical vapor deposition (it is well worth noting that the marked particles were from small particles of commercial cathode or carbon black as conductive agent in the electrodes). To increase purging time to 10 s, the amount of small particles decreased, which indicates that the prolonged purging time could help decrease the precursor condensed on the $LiCoO_2$ cathode. Further prolonging purging time up to 20 s, as a result, few small particles were deposited during the ALD process. Therefore, in this study, the purging time was set as 20 s or longer. Longer purging time could weaken or avoid precursor condensation on the cathode. Therefore, the deposition of TiO_2, ZrO_2 and Al_2O_3 was performed by using sequence of 2 (TTIP) – 20 – 1 (H_2O) – 20, 0.5 ($Zr(NMe_2)_4$) – 30 – 1 (H_2O) – 30, and 0.5 (TMA) – 20 – 1 (H_2O) – 20, respectively. ALD cycles were varied from 2, to 5, 10 and 50 in order to design different coating layer thickness on the cathode electrodes. The metal oxide ZrO_2 thin film was also coated on $LiCoO_2$ powder by the similar process for the comparison.

2.3. Characterization of the coated $LiCoO_2$ electrodes

X-Ray powder diffraction (XRD) patterns were collected on a Bruker D8 Discover Diffractometer using Co Ka radiation (λ = 1.78897 nm) at 40 kV and 100 mA. The morphologies and structures of various metal oxide thin film coating layers were observed by a field emission scanning electron microscope (FE-SEM, Hitachi S-4800), transmission electron microscopy (TEM, Hitachi H-7000), and high-resolution transmission electron microscope (HRTEM, JEOL 2010 FEG). The Zr and Ti K-edge X-ray absorption near edge structure (XANES) spectroscopy were obtained on the Soft X-ray Micro-characterization Beamline (SXRMB, $\Delta E/E$: $\sim 10^{-4}$) at the Canadian Light Source (CLS), a 2.9 GeV third generation synchrotron source, using an InSb(111) and Si (111) double crystal monochromator. The Al K-edge spectra were obtained on the High Resolution Spherical Grating Momochromator (SGM). XANES were recorded in total fluorescence yield (FLY). Data were first normalized to the incident photon flux I_0 measured with an ion chamber. After background correction, the XANES were then normalized using the Athena program.

2.4. Electrochemical testing of the coated $LiCoO_2$ electrodes

CR-2032-type coin cells were assembled in a glove box (Vacuum Atmosphere Company) under a dry argon atmosphere (moisture and oxygen level less than 1 ppm). The ALD coated electrodes and the lithium foils were used as the working electrodes and the counter electrodes, respectively. The electrolyte was composed of 1 M $LiPF_6$ salt dissolved in ethylene carbonate (EC):diethyl carbonate (DEC):ethyl methyl carbonate (EMC) of 1:1:1 volume ratio. Cyclic voltammetry and electrochemical impedance spectroscopy tests were performed on a versatile multichannel potentiostat 3/Z (VMP3). Charge–discharge characteristics were galvanostatically tested between 3.0 and 4.5 V (vs. Li/Li^+) at room temperature using an Arbin BT-2000 Battery Tester. The cells were designed to measure the amount of Co dissolution into the electrolyte as below: (a) the cells were charged to 4.5 V; (b) the cells were carefully disassembled in the glove box; (c) $LiCoO_2$ electrode were stored in the electrolyte at 60 °C for 14 days; (d) the amount of Co content in the electrolyte was measured by inductively coupled plasma atomic absorption spectroscopy (ICP-AAS).

3. Results and discussion

Fig. 1a compares the XRD pattern of pristine $LiCoO_2$ electrode with the coated $LiCoO_2$ electrodes by TiO_2, ZrO_2, and Al_2O_3. Obviously, in all XRD patterns, the reflection peaks originating from $LiCoO_2$ (003), (101), (006), (012), (104), (015), (009), (107), (018), (110), (113), and (021) planes marked can be observed, which shows that the coated cathode electrodes are still indexed to the pure $LiCoO_2$ with the R3m symmetry (JCPDS PDF NO. 44-145). It should be noted that due to some overlap of diffraction peaks (see Fig. S3) of the Al current collector with those of the $LiCoO_2$ cathode, some planes (such as (006), (012), (104), (009), (018), (113), and (021)) from $LiCoO_2$ show higher intensity. More importantly, the reflection peaks corresponding to $LiCoO_2$ does not alter after various metal oxide coatings, in addition, there were no new phase peaks disclosed, indicating that the ALD process has no effect on the cathode crystal structure. In this study, ALD temperatures, i.e., 85 °C, 100 °C, and 150 °C, were used to deposit the amorphous metal oxide thin films on $LiCoO_2$ cathodes. It was reported that the coating layers can react with $LiCoO_2$ at high temperature (600 °C) to form solid solutions on the surface of the cathodes [47]. But, in this study, the ALD deposition temperatures were only 150 °C at most excluding the possibility to form the solid solution on the cathodes, as demonstrated in XRD patterns. On the other hand, the absence of diffraction patterns related to TiO_2, ZrO_2, and Al_2O_3 coatings is due to two facts. One is that the coating layer on the cathode electrodes exists as an amorphous phase. As we reported previously [42,48], an ALD technique is capable of tailoring the crystallinity of deposited metal oxides by controlling deposition temperature. Another fact is due to the ultra-thin nature of the coating layers on the cathode electrodes, ranging from several nanometers to sub-nanometers. Based on the ALD mechanism, the thickness of coating layers increased with number of cycles. For example, a broad pattern at around 37° was observed, corresponding to the amorphous ZrO_2 deposited after 100 ALD cycles (see Fig. S4 in Supplementary data).

XANES is an elemental and absorption edge specific technique that can be used as a finger print analysis. XANES analyses at the Ti, Zr, and Al K-edge were carried out to investigate the local structure of the coating layers, and they further confirmed the formation of various metal oxide layers on the electrodes. Representative spectra are shown in Fig. 1b–d for TiO_2, ZrO_2, and Al_2O_3 coatings by 50 ALD cycles. The spectra of the standard TiO_2, ZrO_2, and Al_2O_3 are also shown for comparison. One can observe six main features related to the standard TiO_2 materials in Fig. 1b due to electronic transition to unoccupied high-energy states near the Fermi level. They are sensitive to the local geometry of the probe Ti atom [49], which is in good agreement with the published data [50]. The coating layer shows the similar peaks to the standard TiO_2, indicating the TiO_2 deposition on $LiCoO_2$ cathode by the ALD process. Similarly, in the case of the Zr and Al K-edge absorption spectra, some distinctive absorption peaks can be observed. The comparison in Fig. 1c and d also suggest the successful deposition of the ZrO_2 and Al_2O_3 coating layers on $LiCoO_2$ cathode. From the above discussion, it can be concluded that various amorphous metal oxide coating layers were successfully deposited on $LiCoO_2$ cathode via an ALD process, which exhibits an advantage of precisely controlling the amorphous nature of the coating layer thickness on the cathodes by suitably adjusting ALD deposition temperatures.

In this study, commercial $LiCoO_2$ cathode with micron-size was used as the target material for coating three metal oxide coating layers via ALD with a series of cycles (2, 5, 10, and 50). The size of commercial secondary $LiCoO_2$ particle is in a range of 3–10 um, consisting of many primary particles with a size of 600 nm–3 um (see Fig. S1 in Supplementary data). Fig. 2a shows a typical high-magnification SEM image of commercial $LiCoO_2$. Obviously, its surface is relatively smooth, being a characteristic of pristine $LiCoO_2$ particle. After an ALD process was performed on this cathode, in contrast, the surface morphology of $LiCoO_2$ cathode showed a little

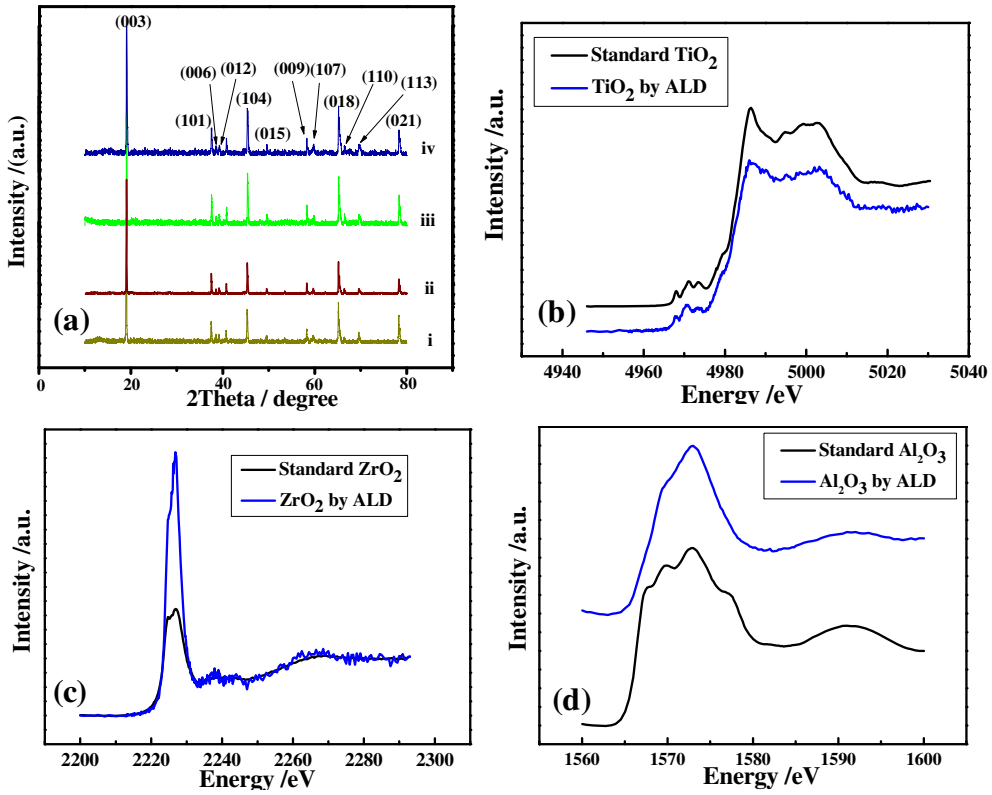

Fig. 1. (a) XRD patterns of (i) the pristine $LiCoO_2$ electrode and the $LiCoO_2$ electrodes coated by various metal oxides with 50 ALD cycles: (i) TiO_2, (ii) ZrO_2, and (iii) Al_2O_3; (b) Ti, (c) Zr, and (d) Al K edge structure in TiO_2, ZrO_2, and Al_2O_3 coatings in $LiCoO_2$ cathode.

bit of change. As shown in Fig. 2b–i, in all the cases, an obvious coating layer can be observed on the surface of $LiCoO_2$ electrode. Additionally, the coating layers differ in their thicknesses on $LiCoO_2$ electrodes. As demonstrated in the previous research work in our group [42], the ALD-resultant metal oxide layers increase with ALD cycles, offering the excellent advantage of precisely controlled coating layer thickness on the cathodes by adjusting ALD deposition cycles. More importantly, a very uniform and dense coating

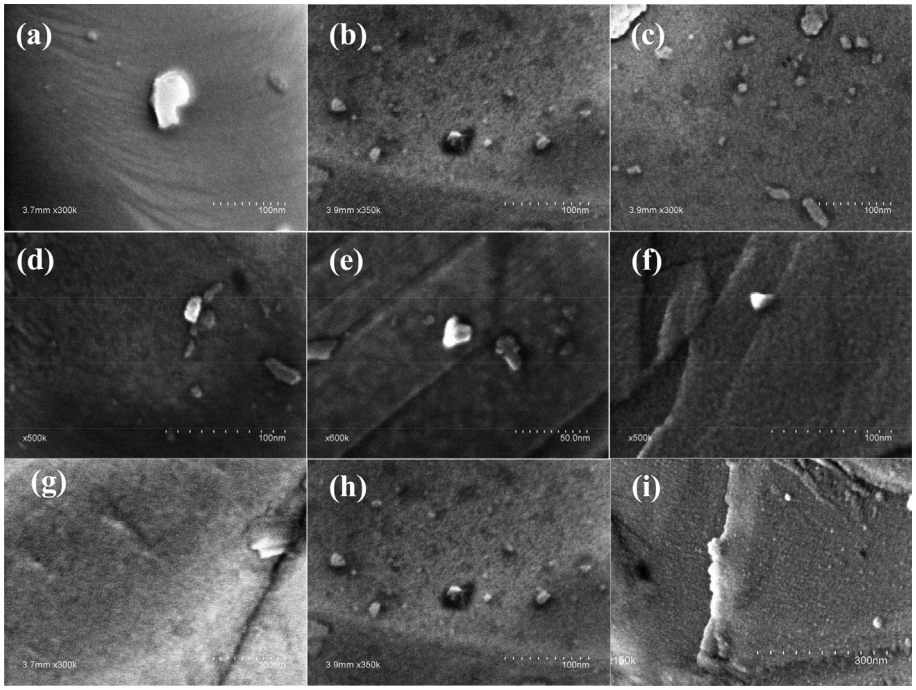

Fig. 2. Typical morphologies of (a) the pristine $LiCoO_2$ electrode and the $LiCoO_2$ electrodes coated by various metal oxides with different ALD cycles: (b) Al_2O_3-5, (c) Al_2O_3-10, (d) TiO_2-5, (e) TiO_2-10, (f) TiO_2-50, (g) ZrO_2-2, (h) ZrO_2-5, and (i) ZrO_2-50.

layer can be observed for these three metal oxides, showing another superiority in ALD-derived coating layers on the cathode electrodes. Fig. 3a–i shows elemental mapping studies on $LiCoO_2$ electrode coated by ZrO_2 with different ALD cycles (2, 10, and 50). The related SEM images are presented in Fig. S5 a–c in Supplementary data. It is clear that the presence of Co and O are homogenous within $LiCoO_2$ cathode, and the ZrO_2 coating layer is uniformly distributed on the surface of $LiCoO_2$ cathode. Similarly, ALD technique produced uniform TiO_2 and Al_2O_3 coating layers on the cathode electrodes (see Fig. S6 and S7 in Supplementary data).

20 mg of the coated $LiCoO_2$ cathodes by ZrO_2 and Al_2O_3 metal oxides were dissolved into a mixture solution of HNO_3 and HCl (*v*:*v*, 1:3) for 24 h. Obtained 1 mL solution further diluted to 9 mL DI water was measured by inductively plasma-atomic absorption spectroscopy (ICP-AAS) to determine the content of ZrO_2 and Al_2O_3 metal oxides in the composite cathodes. The results are shown in Table S1. As expected, the content of both coatings in the coated cathodes increases with ALD cycles, which reveals that the thickness of the coating layers increases when ALD cycles are prolonged during the ALD process. To further quantify the amount of metal oxides deposited, we tested EDX of three metal oxides coated

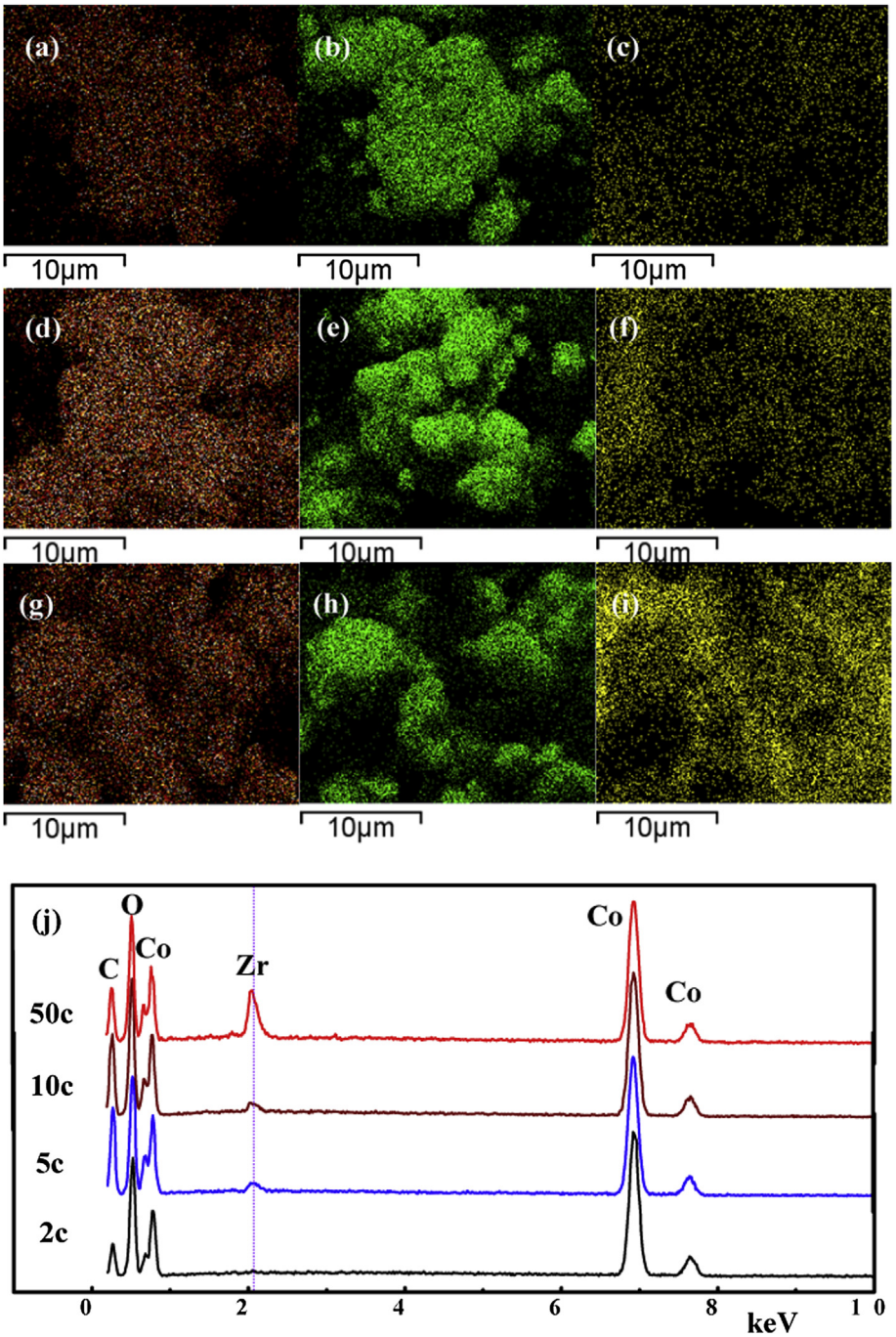

Fig. 3. Elemental mapping of the $LiCoO_2$ electrode coated by ZrO_2 with different ALD cycles: 2 (a–c), 10 (d–f), and 50 (g–i). Elemental mappings of Co (a, d, g), O (b, e, h), and Zr (c, f, i) are shown for each class. The comparison of EDX signals for different ALD coating is shown in Fig. 3j.

$LiCoO_2$ cathode, and compare the change of atomic ratio between metal (Ti, Zr, and Al) and Co with the increase of ALD cycles. In the EDX spectra in Fig. 3j and Fig. S8, the Zr, Al, Ti signals result from the metal oxide coating layers on the $LiCoO_2$ electrode. Moreover, the intensity of the peaks of Zr, Al, Ti become stronger with increased ALD cycles, in good agreement with the results of ICP-AAS. In a case of the atomic ratio of metal (Ti, Zr, and Al) and Co, the value always enhances with increased ALD cycles (see Table S2), being an obvious evidence of the thickness increase of the coating layers with ALD cycles. The thickness evolution of the ZrO_2 coating layers resulting from different ALD cycles was studied by the TEM technique (see Fig. S9 in Supplementary data). It is visible that the increase of the ALD cycles results in smooth and uniform coating layers with higher thickness. Clearly, it indicates the thickness evolution of the coating layers with ALD cycle: the higher the ALD cycle number, the thicker the coating layer is. Therefore, it can be concluded that the amount of metal oxides deposited increases when the ALD cycles increase.

HRTEM was performed to further confirm the coating layers on $LiCoO_2$ electrodes. From HRTEM images, it is possible to evaluate the coating layer thickness on the cathodes (see Fig. 4a–c). In a case of TiO_2 coating, the obtained thickness is around 5.6 nm for 50 ALD cycles based on HRTEM image of Fig. 4a. ALD rate of TTIP–H_2O system depends on a lot of deposition parameters (such as temperature, substrate type and total surface area) [51]. It was reported that when TTIP and water are employed in an ALD reaction below 200 °C, the resultant insufficient reactivity of one precursor water with TTIP could lead to deviations from the self-limited TiO_2 deposition from two ALD precursors. But, adsorption of TTIP on the formed TiO_2 surface is a self-saturated process, as a result, at low deposition temperature, the growth rate of TiO_2 increases as high as 1.5 Å $cycle^{-1}$ [51,52], which is the main reason that in this study TiO_2 deposition rate is beyond the typical growth (around 0.6 Å $cycle^{-1}$ [53]). In Fig. 4b and c, the thickness of ZrO_2 and Al_2O_3 coating layers on $LiCoO_2$ cathode is 6.4 and 6.6 nm, respectively, which is in good agreement with the references [54,55]. The results in Fig. 4a–c clearly reveal that the ALD technique is capable of depositing ultra-thin metal oxide coating layers to completely cover $LiCoO_2$ cathode; moreover, the coating layer thickness can be precisely tuned by controlling ALD cycles. Al_2O_3 was also coated on Si nanowire by the same procedure with 20 ALD cycles, and the resultant HRTEM image is shown in Fig. S10, where a 2.6 nm thickness of Al_2O_3 layer on Si nanowire is clearly observed. The obtained thickness is comparable of one for Al_2O_3 coated $LiCoO_2$ (6.6 nm from 50 ALD cycles), which is in good agreement with the reference [55]. This reveals that ALD mainly dominated the

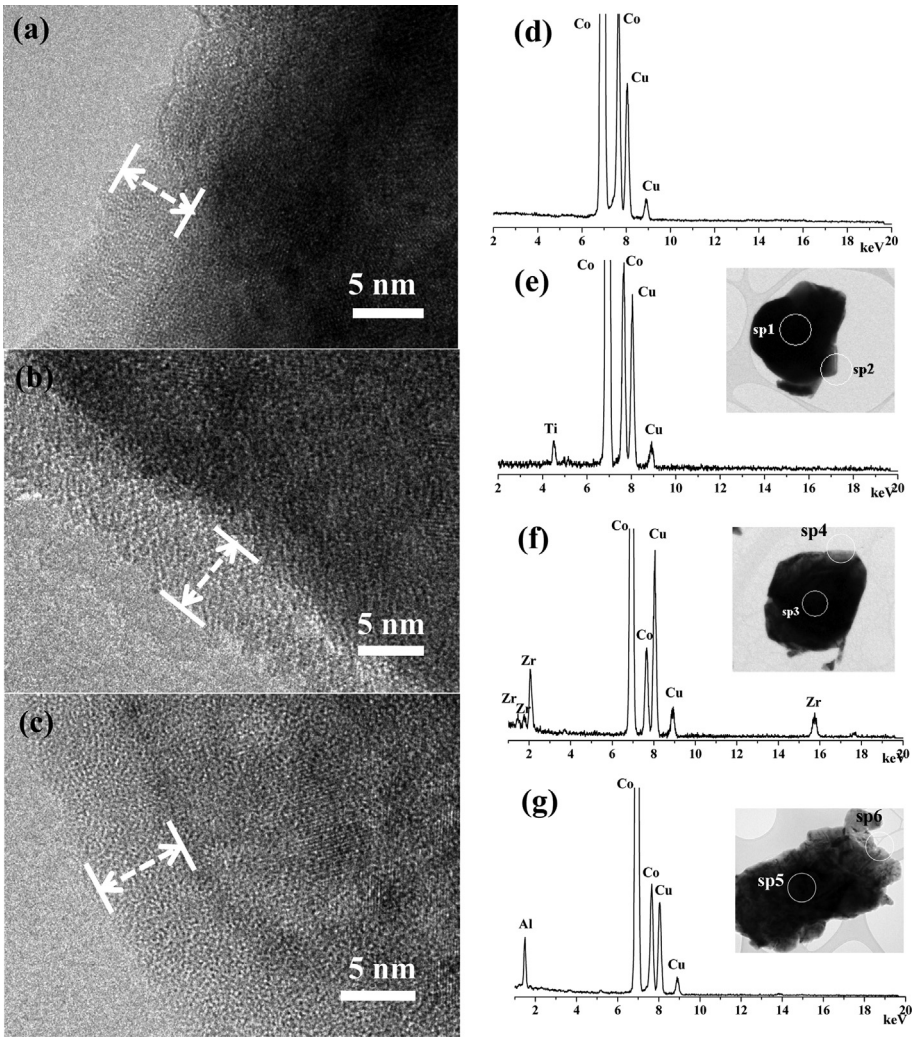

Fig. 4. HRTEM images of the $LiCoO_2$ cathodes by 50-ALD-cycles coating layers: (a) TiO_2, (b) ZrO_2, and (c) Al_2O_3; The EDX signals of different areas labeled as (d) sp1, sp3, sp5, (e) sp2, (f) sp4, and (g) sp6.

deposition process in our ALD chamber. High resolution EDX analysis was performed to further confirm the existence of various metal oxide coating layers on $LiCoO_2$. The different locations labeled sp1–6 were examined to demonstrate the elemental distribution. The locations at sp1, 3, and 5 result in the similar EDX spectra as shown in Fig. 4d, where the strong Co peak is from the cathode, and the Cu signal is due to the grid of HRTEM samples. In Fig. 4e, a Ti peak exists corresponding to location sp2, which indicates a TiO_2 coating layer on $LiCoO_2$. Similarly, Fig. 4f and g shows obvious evidence of other coating layer existence (say ZrO_2 and Al_2O_3).

Fig. 5a shows the typical cyclic voltammograms (CVs) obtained from pristine $LiCoO_2$ electrode at a scan rate of 0.1 mV s^{-1} in a voltage range of 3.3–4.5 V. Clearly, there are three pairs of well defined current peaks (A/A′, B/B′, and C/C′) corresponding to the oxidation and reduction reactions, which are positioned at (4.069/3.795 V), (4.127/4.015 V), and (4.212/4.143 V) in the first scan, respectively. The first pair of redox peaks, (4.069/3.795 V), result from the redox process of Co^{3+} to Co^{4+} for the first-order phase transformation (Li^+ extraction/insertion into $LiCoO_2$ cathode) between two hexagonal phases [56]. Another two pairs of peaks, (4.127/4.015 V), and (4.212/4.143 V), are due to the order–disorder phase transformation between hexagonal and monoclinic phases [57,58].

As shown in Fig. 10a, metal oxide coatings via ALD can be totally covered on $LiCoO_2$ powder, as a result, lithium diffusion and electron transport through the coating layers can slow down due to the poor conductivity of the metal oxides. However, if ALD process is directly applied on $LiCoO_2$ electrode, the situation is different because the metal oxides were not deposited on the contacting area between $LiCoO_2$ particles and the carbon black as the conductive agent (or the current collector). As a result, the electrically insulating coating layers do not destroy the original electrical pathways in the cathode electrodes, where the coated $LiCoO_2$ electrode still keeps electrical conductive network among $LiCoO_2$ particles [33,59]. To compare CV curves of these two types of coatings on $LiCoO_2$ in Figs. 5b and 6e demonstrates that these two coatings can strongly affect lithium extraction from $LiCoO_2$. By contrast, ZrO_2 coated $LiCoO_2$ powder shows an obvious difference during the first two charge processes, which indicates that a big irreversible process occurs in the first charge process due to ZrO_2 coating on $LiCoO_2$ powder. Fig. 5c compares the cycling performance of pristine $LiCoO_2$, ZrO_2 coated $LiCoO_2$ powder and ZrO_2 coated $LiCoO_2$ electrode. Different irreversible capacity can be observed in the inset of Fig. 5c, where ZrO_2 coated $LiCoO_2$ powder shows higher irreversible capacity than the other two cathodes. Moreover, the three cathodes differ in their electrochemical cycling performance. The capacity loss after 100 cycles is 29%, 31%, and 19% for pristine $LiCoO_2$, ZrO_2 coated $LiCoO_2$ powder and ZrO_2 coated $LiCoO_2$ electrode, respectively. As expected, coated $LiCoO_2$ electrode shows higher capacity retention than the pristine one. Oppositely, coated $LiCoO_2$ powder shows poorer cycling performance than the pristine one. Their rate capability is shown in Fig. 5d. During the current density increase from 100 to 700 mA g^{-1}, the coated electrode always shows much higher energy capacities than the coated powder. As we discussed above, in the case of the coated cathode powder, ALD is capable of depositing uniform dense coating layers with poor conductivity on the cathode particles. These coatings significantly decreased lithium diffusion and electron transport in the cathode particles; as a result, it is reasonable that the coated cathode powder shows lower performance than the pristine one. From this point, we mainly focused on various metal oxide coatings on $LiCoO_2$ electrode in the following discussion.

In order to study how the various coating layers affect lithium storage of $LiCoO_2$, the cathode electrodes coated by TiO_2, ZrO_2, and Al_2O_3 were examined by cyclic voltammetry, yielding CV curves (see Fig. 6a–i). One can see that coated $LiCoO_2$ cathodes exhibit similar Li^+ extraction/insertion behaviors as the pristine one does.

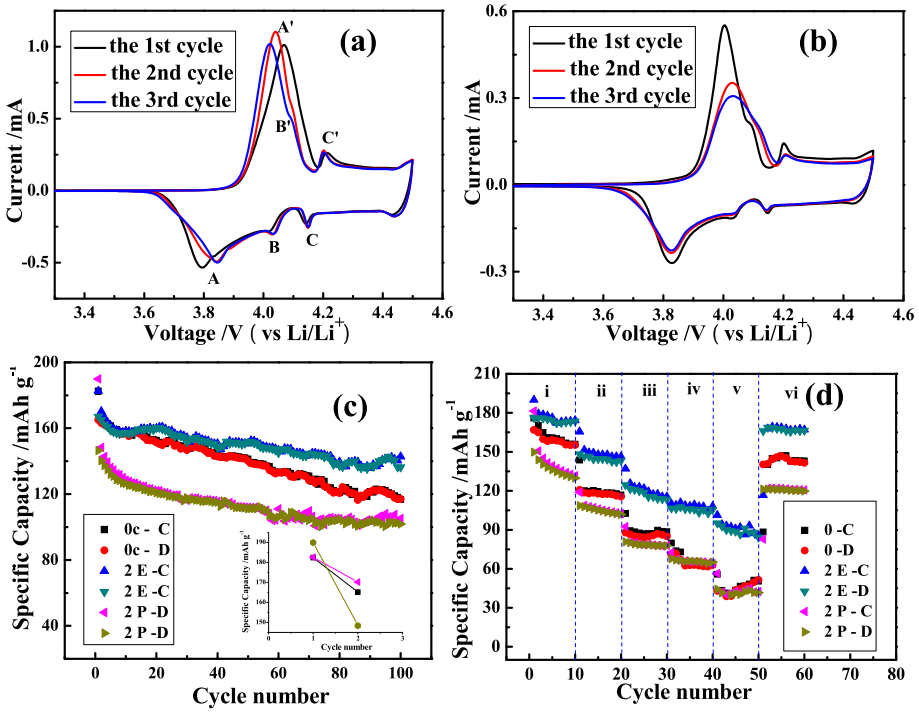

Fig. 5. Cyclic voltammograms of (a) the pristine $LiCoO_2$ and (b) the ZrO_2 coated $LiCoO_2$ powder with 2 ALD cycles (2 P); the comparison of (c) the cycling performance and (d) the rate capability ((i) 100, (ii) 300, (iii) 500, (iv) 600, (v) 700 and (vi) 100 mA g^{-1}) for three cathodes: the pristine $LiCoO_2$, the ZrO_2 coated $LiCoO_2$ powder with 2 ALD cycles, and the ZrO_2 coated $LiCoO_2$ electrode with 2 ALD cycles (2 E).

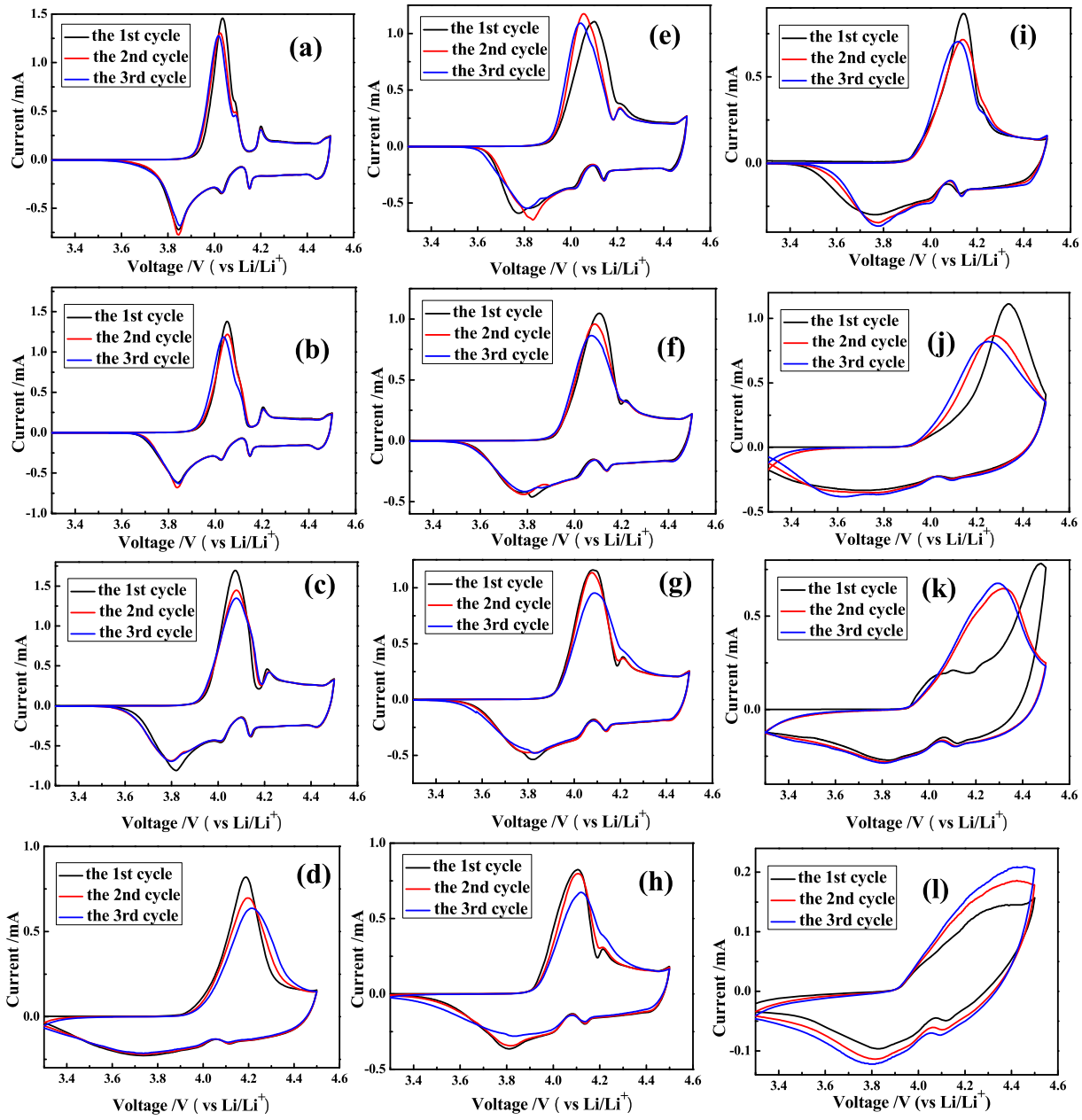

Fig. 6. Cyclic voltammograms of the $LiCoO_2$ electrodes coated by various metal oxides with different ALD cycles: (a) TiO_2-2, (b) TiO_2-5, (c) TiO_2-10, (d) TiO_2-50, (e) ZrO_2-2, (f) ZrO_2-5, (g) ZrO_2-10, (h) ZrO_2-50, (i) Al_2O_3-2, (j) Al_2O_3-5, (k) Al_2O_3-10, and (l) Al_2O_3-50.

However, it is clear that the oxidation and reduction peaks obviously move for ultra-thin coating layers on the electrodes, resulting in different hysteresis (ΔV) between the anodic and cathodic peak voltages. The detailed values were comparatively summarized in Table 1. $LiCoO_2$ cathodes coated by TiO_2 with 2 and 5 ALD cycles show lower ΔV than the pristine cathode. With increasing ALD cycles, the cathodes exhibit higher ΔV. However, ZrO_2 and Al_2O_3 coatings exhibit higher ΔV with all ALD cycles. In contrast, the ΔV of the Al_2O_3 coating is much higher than those of the other two. The different behaviors might stem from two aspects: different electrical conductivity and various deposition rate for coating layers on the cathode.

The cycling performance of $LiCoO_2$ electrodes with and without coating layers was studied in a voltage range of 3.3–4.5 V at a constant current density of 140 mA g^{-1} at room temperature. Fig. 7a–c shows the cyclability of $LiCoO_2$ electrodes coated by TiO_2, ZrO_2, and Al_2O_3, respectively. As it is shown, three types of metal oxide coatings significantly affect the energy capacities and the cycling performance of $LiCoO_2$ cathode: (1) The TiO_2 coating layers by 2, 5, and 10 ALD cycles could increase the specific capacities of $LiCoO_2$ electrode, while further increasing ALD cycles up to 50 worsens the cycling stability; (2) The ZrO_2 coating layers exhibit a bit difference with respect to the TiO_2 ones: 2 and 5 ALD cycle coatings produced positive effect, but negative effect from 10 to 50 ALD cycles; (3) Similar trends were observed with the Al_2O_3 coated cathodes as the ZrO_2 coated ones but Al_2O_3 coatings show better performance. Noteworthily, there was no capacity obtained from $LiCoO_2$ cathode when it was coated with a 50-ALD-cycle Al_2O_3 film. The pristine $LiCoO_2$ cathode delivers a reversible capacity of 165.1 mAh g^{-1} in the 100th cycle, but the capacity retention is only 70.9%. In comparison, the thinner TiO_2 coating layers (2, 5, and 10 ALD cycles), ZrO_2 coating layers (2 and 5 ALD cycles), Al_2O_3 coating

Table 1
The potential of the oxidation and reduction peaks in the first three cycles for the $LiCoO_2$ electrodes coated by various metal oxides with different ALD cycles.

Coatings	ALD cycles	1st scan		2nd scan		3rd scan		Average		
		O	R	O	R	O	R	O	R	ΔV
Pristine		4.069	3.794	4.041	3.842	4.021	3.845	4.044	3.827	0.217
TiO_2	2	4.035	3.845	4.025	3.846	4.017	3.852	4.025	3.848	0.178
	5	4.049	3.836	4.051	3.837	4.035	3.843	4.045	3.839	0.206
	10	4.070	3.818	4.076	3.798	4.077	3.798	4.075	3.805	0.270
	50	4.184	3.740	4.193	3.741	4.215	3.742	4.197	3.741	0.456
ZrO_2	2	4.099	3.779	4.055	3.814	4.041	3.837	4.065	3.810	0.255
	5	4.105	3.825	4.085	3.822	4.072	3.819	4.087	3.822	0.265
	10	4.080	3.820	4.077	3.831	4.088	3.813	4.082	3.821	0.260
	50	4.104	3.808	4.107	3.817	4.119	3.824	4.11	3.816	0.294
Al_2O_3	2	4.143	3.764	4.139	3.777	4.119	3.777	4.134	3.773	0.361
	5	4.335	3.782	4.272	3.782	4.243	3.636	4.283	3.783	0.500
	10	4.475	3.836	4.323	3.820	4.294	3.814	4.364	3.823	0.541
	50	4.342	3.833	4.407	3.824	4.429	3.806	4.393	3.821	0.572

layers (2 and 5 ALD cycles) are capable of improving the cycling performance. However, any further thicker ALD coatings of the three metal oxides inhibit the cycling performance. It is worth noting that the thinnest coatings of the three metal oxides due to 2 ALD cycles commonly improve the resultant $LiCoO_2$ cathodes with the best capacity retention. Fig. 7d compares the capacity retention for these three coating layers. For Al_2O_3 coating, the capacity fade mainly happened in the initial 10 charge/discharge cycles, while the other two coatings show the continuous capacity fade up to the 100th cycle. Obviously, the Al_2O_3 coating layer exhibits the best capability in sustaining $LiCoO_2$ stability. After 100 charge/discharge cycles, the capacity retention of TiO_2, ZrO_2, and Al_2O_3 coated $LiCoO_2$ electrodes is 81.6%, 83.5%, and 93.9%, respectively. The obtained results indicate that surface modification via ultra-thin Al_2O_3 coating layer is an facile but effective strategy to improve the cycling stability of $LiCoO_2$ electrode under high charge cut-off voltage (3.3–4.5 V).

The RLIB rate performance is of particularly importance because the multifarious applications require high power density (high-rate capability) [60]. The rate capabilities of $LiCoO_2$ electrodes with and without coating layers are shown in Fig. 8a–c, whereby the current densities of up to 700 mA g^{-1} have been employed. The energy capacities of the cathode electrodes gradually decrease with an increase of the current density for all samples, which results from the low diffusion rate of the lithium ions in the cathode electrodes [61,62]. It is clearly observed that these three coating layers on the cathode electrodes show different effects on the rate capability of $LiCoO_2$ cathodes. As seen in Fig. 8a–c, TiO_2 coatings with three ALD cycles (say 2, 5, 10) could increase the rate capability of the $LiCoO_2$ cathode. ZrO_2 coating by 2 ALD cycles is beneficial to enhancing its rate performance, but further thicker ALD coatings inversely decrease its rate performance. Unfortunately, different from TiO_2 and ZrO_2 coatings, Al_2O_3 coating lacks of the ability in increasing the rate performance. The rate capability comparison of $LiCoO_2$

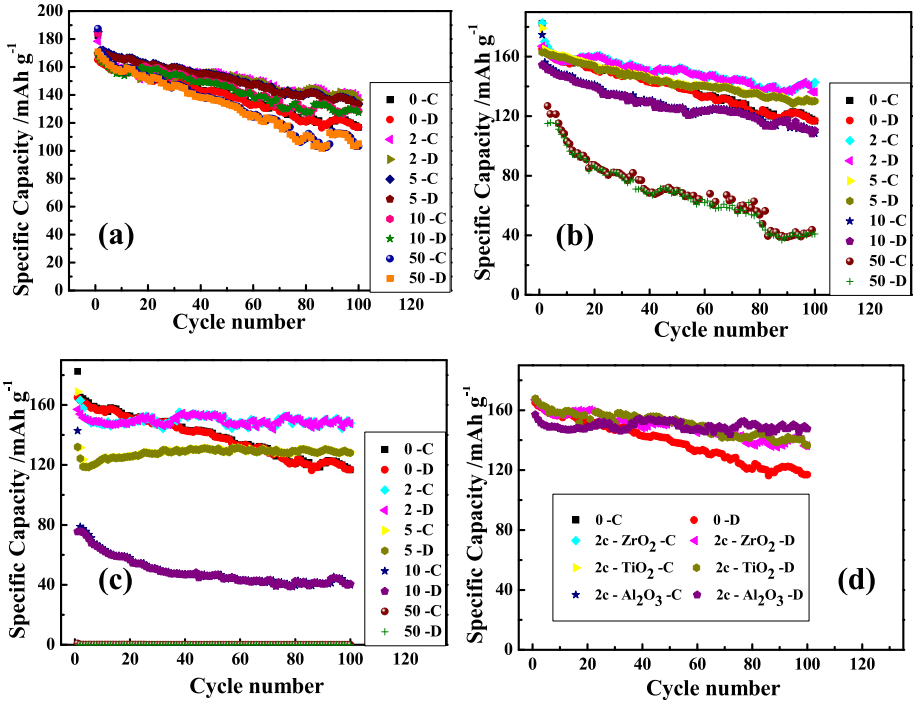

Fig. 7. Reversible charge/discharge capacity verse cycle numbers of the $LiCoO_2$ electrodes coated by metal oxides with different ALD cycles (0, 2, 5, 10, and 50 cycles): (a) TiO_2, (b) ZrO_2, and (c) Al_2O_3; (d) the comparison of cycling performance of $LiCoO_2$ electrodes coated by different metal oxides with 2 ALD cycles.

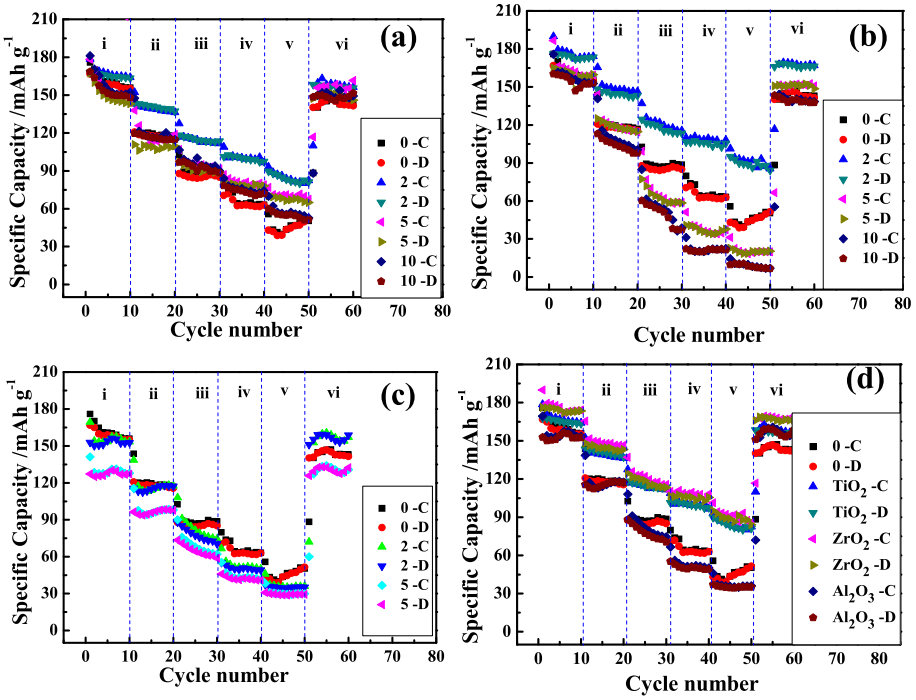

Fig. 8. Rate capability of $LiCoO_2$ electrodes coated by metal oxides with different ALD cycles (0, 2, 5, 10, and 50): (a) TiO_2, (b) ZrO_2, and (c) Al_2O_3 at various current densities: (i) 100, (ii) 300, (iii) 500, (iv) 600, (v) 700 and (vi) 100 mA g^{-1}; (d) the comparison of rate capability of $LiCoO_2$ electrodes coated by different metal oxides with 2 ALD cycles.

electrodes coated by different metal oxides with 2 ALD cycles is shown in Fig. 8d. Different from the result of the cycling performance in Fig. 7d, the ZrO_2 coating could obtain the best effect on the rate capability improvement, while the worst for the Al_2O_3 coating. Obviously, the electrochemical performance of ALD-coated $LiCoO_2$ electrode strongly depends on the type of coating materials that the Al_2O_3 coating shows the best cycling stability while the ZrO_2 coating is capable of obtaining the best rate capability. On the other hand, the ALD-coating effect on nano-sized cathodes is more distinct than that of micron-sized ones [38]. Based on obtained results, further improvement will be expected when these three coating layers are deposited onto nano-sized $LiCoO_2$.

Different electrical conductivity of the coating layers on the cathodes inevitably affects the electrochemical impedance spectroscopy (EIS) when $LiCoO_2$ cathode reacts with lithium, which has an important impact on the battery performance. Fig. 9 shows the EIS of $LiCoO_2$ electrode as well as the influence of TiO_2, ZrO_2, and Al_2O_3 coatings, respectively. All measurements were performed at 3.8 V in the discharge process at different cycles (say the 20th and 50th cycles). The obtained EIS is a collective response of kinetic processes of $LiCoO_2$ reaction with lithium, which consists of two depressed semicircles at high and medium frequency domains, and a line at low frequency region, being in good agreement with previously reported results [63,64]. As shown in Fig. 9a, the EIS of the pure electrode distinctly changes with the charge/discharge cycles, where there is a significant difference between the 20th cycle and 50th cycles. The coated electrodes show little EIS change on cycling. Importantly, it is noticeable that the EIS of Al_2O_3 coated $LiCoO_2$ shows the nearly same trend for the 20th and 50th cycles, but its diameter of two overlapped semicircles has higher value than that of $LiCoO_2$ through these two cycles, which is due to increase of resistance by insulating Al_2O_3 coating layer. The EIS comparison in Fig. 9 obviously shows a protective effect of the coating layers on $LiCoO_2$ electrode surface. A possible equivalent circuit is depicted in the inset of Fig. 9a to simulate $LiCoO_2$ electrode reaction with lithium, where R_e is the ohmic electrolyte resistance; R_{sl} corresponds to the resistance for Li^+ migration through the surface film; C_{sl} denotes interfacial capacitance corresponding to R_{sl}; C_{dl} and R_{ct} are the double-layer capacitance and charge transfer resistance, respectively; and W is the finite-length Warburg impedance that reflects the solid-state diffusion of Li^+ into $LiCoO_2$ cathode [65]. As mentioned, R_{sl} corresponds to the resistance for Li^+ migration through the surface film. Assuming that the surface film is related to ALD derived metal oxide layers, the pristine $LiCoO_2$ without the metal oxide layers would exhibit one semicircles in the EIS. Thus, the surface film corresponds to the solid electrolyte interphase (SEI), which is consistent with the reference [66]. To further confirm it, the EIS under open circuit condition for various cathode electrodes are shown in the inset of Fig. 9. Clearly, the EIS under open circuit condition mainly consist of one semicircle. As it is well known, the SEI could be not formed under open circuit condition. These strongly indicates that R_{sl} corresponds to the resistance for Li^+ migration through the SEI. However, it can be observed that the semicircles corresponding to R_{sl} show some difference in Fig. 9a–d. As previously reported, the SEI on the pristine $LiCoO_2$ originates from the decomposition products of the electrolyte [67]. In the case of $LiCoO_2$ coated by metal oxides, the formed SEI also consists of fluoride metals according to Eqs. (4)–(6) besides the decomposition products of the electrolyte.

$$TiO_2 + 4HF \rightarrow TiF_4 + 4H_2O \quad (4)$$

$$ZrO_2 + 4HF \rightarrow ZrF_4 + 4H_2O \quad (5)$$

$$Al_2O_3 + 6HF \rightarrow 2AlF_3 + 3H_2O \quad (6)$$

Therefore, different components in the formed SEI result in some difference of the semicircles corresponding to R_{sl}.

After simulating by the equivalent circuit in the inset of Fig. 9a, it was found that R_{ct} of $LiCoO_2$ in the 20th cycle is 336 Ω, which is much smaller than in the 50th cycle, i.e., 505 Ω. The electrical conductivity of the coating layers is different from that of $LiCoO_2$

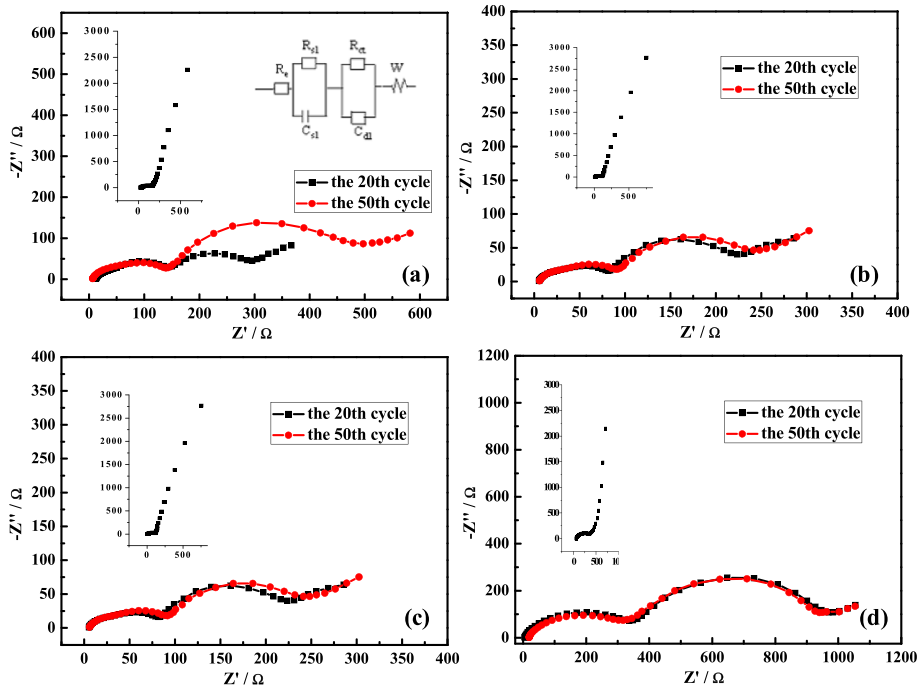

Fig. 9. Electrochemical impedance spectroscopy at 3.8 V in the discharge process of the 20th and 50th cycles for the $LiCoO_2$ electrodes coated by metal oxides with 10 ALD cycles: (a) the pristine $LiCoO_2$, (b) TiO_2, (c) ZrO_2, and (d) Al_2O_3.

cathode, which significantly affects of the charge transfer resistance of the cathode. As a result, TiO_2 coated $LiCoO_2$ shows different R_{ct} in the 20th and the 50th cycle, that is, 81 Ω and 132 Ω, respectively, while 97 Ω and 103 Ω for ZrO_2 coating, respectively. Interestingly, the Al_2O_3 coating exhibits the same R_{ct} value (both are 629 Ω) in the 20th and the 50th cycle, where high R_{ct} results from the low conductivity of Al_2O_3 coating layer. It is obvious that during lithium insertion/extraction processes, R_{ct} of the pristine $LiCoO_2$ continually increases. In the comparison to that of the pristine $LiCoO_2$, R_{ct} of coated $LiCoO_2$ almost keeps stable. The coating layers could reduce the decomposition of the electrolyte on the charged particle surface, moreover, upon cycling they would partially absorb the strain originating from the volumetric change of the granules, which decreases the stress among the binder, the cathode, and the conductive agent, thereby reduce the formation of the voids among them [66]. Therefore, the coating layers are capable of forming a significant protective function on $LiCoO_2$ cathodes. In particular, the Al_2O_3 coating could protect the cathode more effectively from the reactions with the electrolyte during the charge/discharge processes.

As mentioned in the Introduction, an available approach to increase the energy capacity of $LiCoO_2$ is to charge it at higher voltages beyond 4.2 V. However, it was reported that higher voltage charging $LiCoO_2$ would undergo a severe deterioration in the cathode stability, mainly due to three aspects: (1) In the region of higher charging voltage more than 4.2 V, the amount of cobalt dissolution into the electrolyte also increases, resulting in a capacity fading occurred [68]. It is worth noting that the dissolution of $LiCoO_2$ into the electrolyte can be controlled by surface chemical reaction [69]. In this study, three types of metal oxide layers were coated on $LiCoO_2$ electrode, which can serve as an active HF scavenger to decrease the local active concentration of HF acid in the electrolyte near $LiCoO_2$ surface as Eqs. (4)–(6) [7]. As was shown in Fig. 10b, these coatings can keep $LiCoO_2$ particles from direct contact with the HF acid in the electrolyte, prevent the cobalt from dissolution in the electrolyte, thereby increase cycling performance of $LiCoO_2$ electrode. However, the role as HF scavenger might differ among these three coatings. To confirm it, during the electrode storage at 60 °C, the amount of Co dissolution into the electrolyte was tested by ICP-AAS. The amount of pristine $LiCoO_2$ corresponds to approximately 60.3 ppm after 14 days. And the coated $LiCoO_2$ electrodes show a decrease of the Co dissolution into the electrolyte, 15.5, 14.3, and 11.6 ppm for TiO_2, ZrO_2, and Al_2O_3 coatings, respectively. The Al_2O_3 coating more significantly decreases the Co dissolution in comparison to other two coatings (see Fig. 10b). (2) As Wang et al. reported, the electrons in the conduction band of $LiCoO_2$ flows into the metal oxide coatings if the conduction band minimum of the cathode is more than those of the metal oxides, which results in the metal oxide coatings undergoing a redox reaction [37]. As a result, the electrical band structure of various metal oxides has an important influence on $LiCoO_2$ performance. In this study, the charge cut-off voltage range is 3.3–4.5 V, the metal oxide coatings on the cathode electrodes could show the band gap energy more than $4.5 - 3.3 + 2.4 = 3.6$ eV (E_g of $LiCoO_2$ is 2.4 eV) to avoid the reduction of the metal oxide coatings [37]. The band gap energy (E_g) of TiO_2, ZrO_2, and Al_2O_3 is 3.18, 5.80, and 9.00 eV, respectively [37,70]. Therefore, the Al_2O_3 coating provides the best cycling stability, while the worst for the TiO_2 coating. (3) The Co dissolution into the electrolyte is coupled with the release of lithium and oxygen with the structural degradation of $LiCoO_2$ cathode [68]. The CV curves of $LiCoO_2$ cathode could provide some information for the phase transition. As shown in Fig. 5a, an anodic peak located at 4.212 V corresponding to the hexagonal-monoclinic phase transition can be obviously observed when the cathode is charged beyond 4.2 V, which is good agreement with the references [71,72]. After coating various metal oxides by ALD, as shown in Fig. 6, the coated cathodes show different behaviors in occurring this phase transition. In Fig. 6a–d, the TiO_2 coating layers still show this anodic peak above 4.2 V, having no effect on this phase transition, while the decrease of the peak intensity indicates that the ZrO_2 coating layers can decrease this phase transition (Fig. 6e–h). Interestingly, no anodic peak above 4.2 V could be found for the

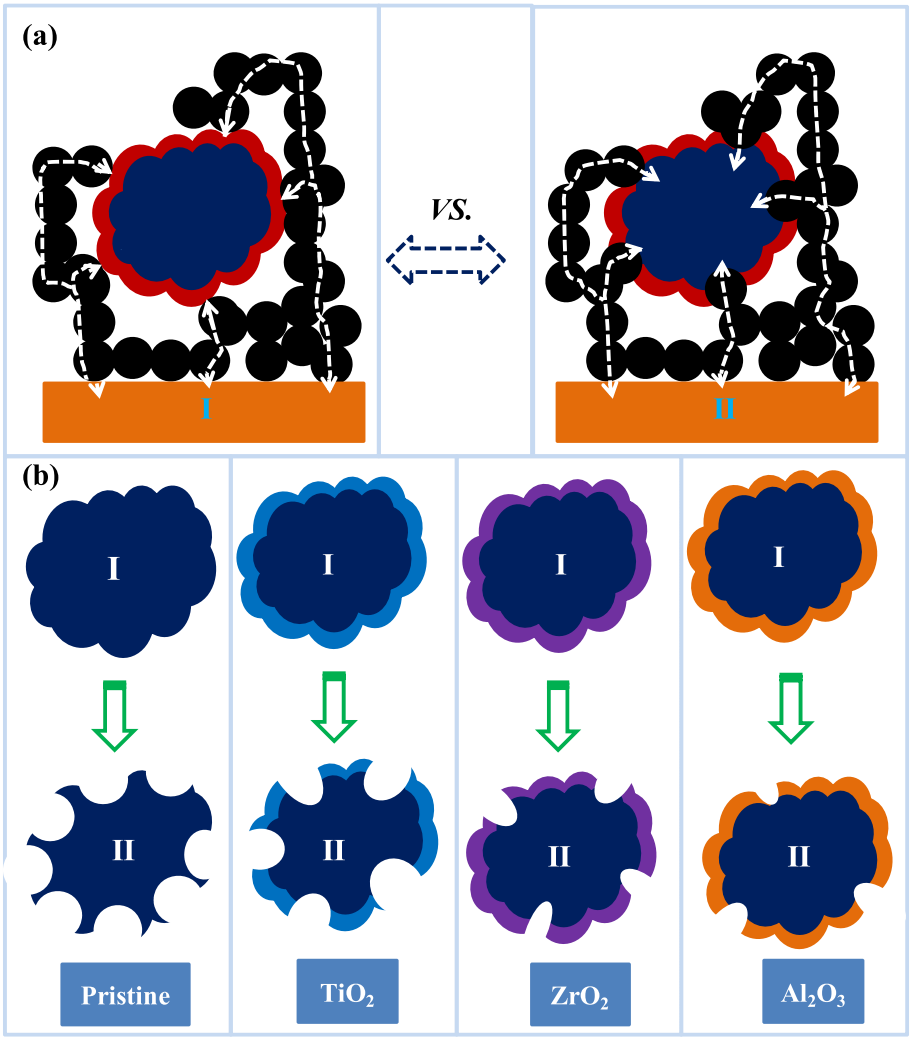

Fig. 10. (a) Schematic illustration of ALD coating powders (I) vs. electrodes (II) of the cathodes; (b) comparison of Co dissolution of $LiCoO_2$ with various coating layers before (I) and after (II) cycles.

Al_2O_3 coating $LiCoO_2$, which demonstrates that the Al_2O_3 coating layers suppress this phase transition during repeated cycles. These phenomena are in good agreement with the EIS results in Fig. 9, where the suppression of the phase transition results in little change of EIS with cycle increase. (3) When the cathode $Li_{1-x}CoO_2$ is charged up to $x = 0.5$ (the cutoff voltage is 4.2 V), it can undergo the hexagonal-monoclinic-hexagonal phase transition accompanied by the lattice expansion (~2.6%) in the *c*-direction [71–74]. Increasing the cutoff voltage up to 4.5 V, the high variation of *c* axis is no longer negligible that an abrupt shrinkage along the *c*-axis direction corresponds to ~9.0% volume change, accompanying a cation disorder which causes a portion of lithium ion to enter the 3b sites of Co [75]. Moreover, the *c*-axis shrinkage causes some cracks within $LiCoO_2$ particles as well as a loss of electrical contact between the cathodes and the conductive additives or the electrode current collector or both [48,72,76], which results in cycle degradation. The metal oxide coating layers employed have different fracture toughness resulting in various mechanical behaviors on $LiCoO_2$ cathode upon repeated cycling, in the order of $ZrO_2 > Al_2O_3 > TiO_2$ [77], resulting in different behavior in increasing the structural stability of $LiCoO_2$ cathode. Based on above discussion, the Al_2O_3 coating layer could show the best behavior in increasing cycling performance (at 140 mAh g^{-1}) of $LiCoO_2$ cathode. However, due to the larger electrochemical polarization of the Al_2O_3 coating layer, the supply of electrons becomes problematic. As a result, the Al_2O_3 coating layer is not capable of increasing rate capability of the cathodes, oppositely, its existence as a coating layer decreases the rate capability in comparison to the pristine $LiCoO_2$ cathode. In contrast, the ZrO_2 coating layer with higher electrical conductivity than Al_2O_3 one could show better ability in enhancing rate capability than the other two coatings. Therefore, among three coating materials, the Al_2O_3 coating brings the best cycling performance while the ZrO_2 coating contributes to the best rate capability, which reveals that ALD derived coating materials are functionally specific, and for the best improvement of a cathode, a particular coating material should be sought.

4. Conclusion

In summary, ALD derived surface coatings with various metal oxides are effective to increase the cycling performance and the rate capability of the commercial $LiCoO_2$ cathode in RLIBs. Our results demonstrate that various metal oxide coating layers have different influences on the cycling performance and the rate capability of $LiCoO_2$ electrode: (a) different ALD-cycle deposition could cause some difference in enhancing cycling performance, and 2-ALD-cycle coatings show the best effect; (b) the Al_2O_3 coating

with high band gap energy ($E_g = 9.00$ eV) effectively suppresses the phase transitions during electrochemical cycling, showing better cycling performance than the TiO_2 and ZrO_2 ones, but the worse rate capability from its poor conductivity; (c) the ZrO_2 coating by 2 ALD cycles is better in increasing the rate capability than the TiO_2 and Al_2O_3 ones, but further increasing ALD cycle leads to poorer rate capability in composition to the pristine $LiCoO_2$ cathode. The various behaviors in performance improvement could be attributed to several important roles of these coating layers: (1) electrical conductivity; (2) electrical band structure; (3) suppression of the phase transition; (4) fracture toughness; and (5) scavenging HF species from the electrolyte. Therefore, this study not only demonstrates that an ALD technique is a powerful coating technique to increase the electrochemical performance of the cathodes by surface modification in RLIBs, but also shows that different metal oxide coatings have an important influence on the cathode performance in the RLIB applications. The ultra-thin Al_2O_3 coating layer shows great effectiveness in enhancing cyclic performance, while ZrO_2 coating layer exhibits the best effect on rate capability of $LiCoO_2$ cathode in RLIBs.

Acknowledgments

This research was supported by the Natural Science and Engineering Research Council of Canada (NSERC), General Motors of Canada, Canada Research Chair (CRC) Program, Canadian Foundation for Innovation (CFI), Ontario Research Fund (ORF), Early Researcher Award (ERA) and the University of Western Ontario. X. Li is grateful to Springpower International, Inc. and the MITACS Elevate Strategic Fellowship Program.

Appendix A. Supplementary data

Supplementary data related to this article can be found at http://dx.doi.org/10.1016/j.jpowsour.2013.08.042.

References

[1] M.S. Whittingham, Chem. Rev. 104 (2004) 4271–4301.
[2] A. Manthiram, J. Phys. Chem. Lett. 2 (2011) 176–184.
[3] J.M. Tarascon, Philos. Trans. R. Soc. A 368 (2010) 3227–3241.
[4] K. Mizushima, P.C. Jones, P.J. Wiseman, J.B. Goodenough, Mater. Res. Bull. 15 (1980) 783–789.
[5] A.R. Armstrong, P.G. Bruce, Nature 381 (1996) 499–500.
[6] X. Gu, J.L. Liu, J.H. Yang, H.J. Xiang, X.G. Gong, Y.Y. Xia, J. Phys. Chem. C 115 (2011) 12672–12676.
[7] L. Su, Y. Jing, Z. Zhou, Nanoscale 3 (2011) 3967–3983.
[8] M. Jo, S. Jeong, J. Cho, Electrochem. Commun. 12 (2010) 992–995.
[9] T. Mei, K. Tang, Y. Zhu, Y. Qian, Dalton Trans. 40 (2011) 7645–7650.
[10] H.J. Orman, P.J. Wiseman, Acta Crystallogr. Sect. C Cryst. Struct. Commun. 40 (1984) 12–14.
[11] C. Delmas, C. Fouassier, P. Hagenmuller, Physica B+C 99 (1980) 81–85.
[12] Y. Talyosef, B. Markovsky, R. Lavi, G. Salitra, D. Aurbach, D. Kovacheva, M. Gorova, E. Zhecheva, R. Stoyanova, J. Electrochem. Soc. 154 (2007) A682–A691.
[13] X. Fang, Y. Lu, N. Ding, X.Y. Feng, C. Liu, C.H. Chen, Electrochim. Acta 55 (2010) 832–837.
[14] R. Pitchai, V. Thavasi, S.G. Mhaisalkar, S. Ramakrishna, J. Mater. Chem. 21 (2011) 11040–11051.
[15] K.F. Hsu, S.Y. Tsay, B.J. Hwang, J. Mater. Chem. 14 (2004) 2690–2695.
[16] M. Okubo, E. Hosono, T. Kudo, H.S. Zhou, I. Honma, Solid State Ionics 180 (2009) 612–615.
[17] X.L. Xiao, L.M. Yang, H. Zhao, Z.B. Hu, Y.D. Li, Nano Res. 5 (2012) 27–32.
[18] D.I. Choi, G.B. Han, D.J. Lee, J.K. Park, J.W. Choi, J. Electrochem. Soc. 158 (2011) A1150–A1154.
[19] D. Liu, G. Cao, Energy Environ. Sci. 3 (2010) 1218–1237.
[20] M. Jo, Y.S. Hong, J. Choo, J. Cho, J. Electrochem. Soc. 156 (2009) A430–A434.
[21] N. Andreu, I. Baraille, H. Martinez, R. Dedryvere, M. Loudet, D. Gonbeau, J. Phys. Chem. C 116 (2012) 20332–20341.
[22] L. Dahéron, R. Dedryvère, H. Martinez, D. Flahaut, M. Ménétrier, C. Delmas, D. Gonbeau, Chem. Mater. 21 (2009) 5607–5616.
[23] Y. Takahashi, S. Tode, A. Kinoshita, H. Fujimoto, I. Nakane, S. Fujitani, J. Electrochem. Soc. 155 (2008) A537–A541.
[24] S.T. Myung, K. Amine, Y.K. Sun, J. Mater. Chem. 20 (2010) 7074–7095.
[25] N. Pentyala, R.K. Guduru, P.S. Mohanty, Electrochim. Acta 56 (2011) 9851–9859.
[26] R. Benedek, A. van de Walle, J. Electrochem. Soc. 155 (2008) A711–A715.
[27] D. Aurbach, K. Gamolsky, B. Markovsky, G. Salitra, Y. Gofer, U. Heider, R. Oesten, M. Schmidt, J. Electrochem. Soc. 147 (2000) 1322–1331.
[28] W. Hong, C. Ming-Cai, Electrochem. Solid State Lett. 9 (2006) A82–A85.
[29] Z. Zhang, Z. Gong, Y. Yang, J. Phys. Chem. B 108 (2004) 17546–17552.
[30] B.J. Hwang, C.Y. Chen, M.Y. Cheng, R. Santhanam, K. Ragavendran, J. Power Sources 195 (2010) 4255–4265.
[31] L.L. Chang, Y.N. Wang, X. Zhao, J.C. Huang, Mater. Sci. Eng. A 496 (2008) 512–516.
[32] Y. Bai, Y. Yin, N. Liu, B. Guo, H. Shi, J. Liu, Z. Wang, L. Chen, J. Power Sources 174 (2007) 328–334.
[33] I.D. Scott, Y.S. Jung, A.S. Cavanagh, Y.F. An, A.C. Dillon, S.M. George, S.H. Lee, Nano Lett. 11 (2011) 414–418.
[34] Z.H. Chen, Y. Qin, K. Amine, Y.K. Sun, J. Mater. Chem. 20 (2010) 7606–7612.
[35] C. Li, H.P. Zhang, L.J. Fu, H. Liu, Y.P. Wu, E. Rahm, R. Holze, H.Q. Wu, Electrochim. Acta 51 (2006) 3872–3883.
[36] H. Li, Z. Wang, L. Chen, X. Huang, Adv. Mater. 21 (2009) 4593–4607.
[37] H.M. Cheng, F.M. Wang, J.P. Chu, R. Santhanam, J. Rick, S.C. Lo, J. Phys. Chem. C 116 (2012) 7629–7637.
[38] X.N. Luan, D.S. Guan, Y. Wang, J. Nanosci. Nanotechnol. 12 (2012) 7113–7120.
[39] J.T. Lee, F.M. Wang, C.S. Cheng, C.C. Li, C.H. Lin, Electrochim. Acta 55 (2010) 4002–4006.
[40] Y.S. Jung, P. Lu, A.S. Cavanagh, C. Ban, G.H. Kim, S.H. Lee, S.M. George, S.J. Harris, A.C. Dillon, Adv. Energy Mater. 3 (2013) 213–219.
[41] M. Bettge, Y. Li, B. Sankaran, N.D. Rago, T. Spila, R.T. Haasch, I. Petrov, D.P. Abrahama, J. Power Sources 233 (2013) 346–357.
[42] X. Meng, X.Q. Yang, X. Sun, Adv. Mater. 24 (2012) 3589–3615.
[43] L.A. Riley, A.S. Cavanagh, S.M. George, Y.S. Jung, Y. Yan, S.H. Lee, A.C. Dillon, ChemPhysChem 11 (2010) 2124–2130.
[44] X.C. Xiao, P. Lu, D. Ahn, Adv. Mater. 23 (2011) 3911–3915.
[45] Y. He, X.Q. Yu, Y.H. Wang, H. Li, X.J. Huang, Adv. Mater. 23 (2011) 4938–4941.
[46] Y.S. Jung, A.S. Cavanagh, L. Gedvilas, Adv. Energy Mater. 2 (2012) 1022–1027.
[47] J. Cho, Y.J. Kim, B. Park, Chem. Mater. 12 (2000) 3788–3791.
[48] X. Li, X. Meng, J. Liu, D. Geng, Y. Zhang, M.N. Banis, Y. Li, J. Yang, R. Li, X. Sun, M. Cai, M.W. Verbrugge, Adv. Funct. Mater. 22 (2012) 1647–1654.
[49] H. Jung, S.M. Paek, J.B. Yoon, J.H. Choy, J. Porous Mater. 14 (2007) 369–377.
[50] O.A. Usov, K.Y. Pogrebitskii, B.T. Melekh, Y.N. Yurev, S.A. Song, Phys. Solid State 41 (1999) 811–813.
[51] D.M. King, X. Liang, Y. Zhou, C.S. Carney, L.F. Hakim, P. Li, A.W. Weimer, Powder Technol. 183 (2008) 356–363.
[52] J. Aarik, A. Aidla, T. Uustare, M. Ritala, M. Leskela, Appl. Surf. Sci. 161 (2000) 385–395.
[53] R. Katamreddy, V. Omarjee, B. Feist, C. Dussarrat, ECS Trans. 16 (2008) 113–122.
[54] D.M. Hausmann, E. Kim, J. Becker, R.G. Gordon, Chem. Mater. 14 (2002) 4350–4358.
[55] M.D. Groner, F.H. Fabreguette, J.W. Elam, S.M. George, Chem. Mater. 16 (2004) 639–645.
[56] Y. Gu, D. Chen, X. Jiao, F. Liu, J. Mater. Chem. 17 (2007) 1769–1776.
[57] K. Dokko, S. Horikoshi, T. Itoh, M. Nishizawa, M. Mohamedi, I. Uchida, J. Power Sources 90 (2000) 109–115.
[58] J.N. Reimers, J.R. Dahn, J. Electrochem. Soc. 139 (1992) 2091–2097.
[59] Y.S. Jung, A.S. Cavanagh, L.A. Riley, S.H. Kang, A.C. Dillon, M.D. Groner, S.M. George, S.H. Lee, Adv. Mater. 22 (2010) 2172–2176.
[60] G. Armstrong, A.R. Armstrong, P.G. Bruce, P. Reale, B. Scrosati, Adv. Mater. 18 (2006) 2597–2600.
[61] X. Li, Y. Xu, J. Solid State Electrochem. 12 (2008) 851–855.
[62] X. Li, Y. Xu, Appl. Surf. Sci. 253 (2007) 8592–8596.
[63] Y.K. Sun, J.M. Han, S.T. Myung, S.W. Lee, K. Amine, Electrochem. Commun. 8 (2006) 821–826.
[64] X.F. Li, Y.L. Xu, Electrochem. Commun. 9 (2007) 2023–2026.
[65] X.F. Li, A. Dhanabalan, X.B. Meng, L. Gu, X.L. Sun, C.L. Wang, Microporous Mesoporous Mater. 151 (2012) 488–494.
[66] G. Li, Z.X. Yang, W.S. Yang, J. Power Sources 183 (2008) 741–748.
[67] S. Malmgrena, K. Cioseka, M. Hahlina, T. Gustafssona, M. Gorgoic, H. Rensmob, K. Edström, Electrochim. Acta 97 (2013) 23–32.
[68] G.G. Amatucci, J.M. Tarascon, L.C. Klein, Solid State Ionics 83 (1996) 167–173.
[69] C.K. Lee, K.I. Rhee, Hydrometallurgy 68 (2003) 5–10.
[70] V.V. Afanasev, M. Houssa, A. Stesmans, M.M. Heyns, J. Appl. Phys. 91 (2002) 3079–3084.
[71] E. Plichta, S. Slane, M. Uchiyama, M. Salomon, D. Chua, W.B. Ebner, H.W. Lin, J. Electrochem. Soc. 136 (1989) 1865–1869.
[72] G. Ting-Kuo Fey, C.Z. Lu, T. Prem Kumar, Y.C. Chang, Surf. Coat. Technol. 199 (2005) 22–31.
[73] H. Wang, Y.I. Jang, B. Huang, D.R. Sadoway, Y.M. Chiang, J. Electrochem. Soc. 146 (1999) 473–480.
[74] Z. Wang, C. Wu, L. Liu, F. Wu, L. Chen, X. Huang, J. Electrochem. Soc. 149 (2002) A466–A471.
[75] L.J. Fu, H. Liu, C. Li, Y.P. Wu, E. Rahm, R. Holze, H.Q. Wu, Solid State Sci. 8 (2006) 113–128.
[76] T. Fang, J.G. Duh, S.R. Sheen, Thin Solid Films 469–470 (2004) 361–365.
[77] J. Cho, Y.J. Kim, T.J. Kim, B. Park, Angew. Chem. Int. Ed. 40 (2001) 3367–3369.